IEICE TRANS. COMMUN., VOL.E97–B, NO.2 FEBRUARY 2014

PAPER

SPICE Behavioral Modeling of RF Current Injection in Wire Bundles

Flavia GRASSI[†a)], **Giordano SPADACINI**[†], *Nonmembers*, *and* **Sergio A. PIGNARI**[†], *Member*

SUMMARY In this work, a measurement-based procedure aimed at deriving a behavioral model of Bulk Current Injection (BCI) probes clamped onto multi-wire cable bundles is proposed. The procedure utilizes the measurement data obtained by mounting the probe onto the calibration jig for model-parameters extraction, and 2D electromagnetic simulations to adapt such parameters to the specific characteristics of the cable bundle under analysis. Outcome of the analysis is a behavioral model which can be easily implemented into the SPICE environment. Without loss of generality, the proposed model is here used to predict the radio-frequency noise stressing the terminal units of a two-wire harness. Model accuracy in predicting the common and differential mode voltages induced by BCI at the line terminals is assessed by EM modeling and simulation of the involved injection setup by the commercial software CST Microwave Studio.

key words: *Bulk Current Injection (BCI), conducted immunity, behavioral modeling, SPICE simulation*

1. Introduction

Due to the wide spread of immunity test procedures based on the Bulk Current Injection (BCI) technique, modeling of injection probes for BCI have recently gained increasing attention from the Electromagnetic Compatibility (EMC) community. The final aim is twofold. On the one hand, probe models allowing for accurate prediction in a wide frequency range can be exploited to increase test significance and effectiveness. Indeed, they provide insight to strengthen the correlation between BCI and other susceptibility testing techniques [1]–[3]. On the other hand, they represent time- and cost-effective tools for the EMC-oriented design of complex systems. In line with these needs, in a previous work [4] two different strategies for probe modeling were proposed and validated versus measurement. The first approach involves a circuit representation of the probe interior [see Fig. 1(a)] and resorts to input impedance measurement to characterize the frequency response of the probe ferrite-core, i.e., the frequency-dependent inductances $L_P(\omega)$, $L_W(\omega)$, and $M(\omega)$ in Fig. 1(a). This is carried out in the absence of the wiring harness. Therefore the obtained model does not account for the effects due to probe-to-wire interaction, which shall be *a posteriori* included by recourse to specific circuit elements [i.e., inductance L_d and capacitances C_S in Fig. 1(a)]. Unfortunately, this approach presumes information on the probe interior (geometrical data and material properties) usually not available to the end-user. As a consequence, model extension to injection devices with different characteristics (e.g., bandwidth, number of turns, and dimensions) is not straightforward. Conversely, the second procedure leads to the equivalent circuit in Fig. 1(b). Here, the effects of RF energy transfer and loading exerted by the probe onto the wiring harness are modeled by the circuit elements V_S, Z_P, Y_P whose frequency behavior is retrieved from measurement data. The procedure for parameter extraction is smarter and not affected by the limitations of the previous approach. However, the obtained parameters V_S, Z_P, Y_P are inherently affected by electromagnetic (EM) interaction between the probe and the *ad hoc* fixture used for experimental characterization, [4]. These limitations were overcome in [5], where the calibration jig — i.e., a standard EMC equipment — instead of the *ad hoc* fixture in [4] was used for experimental characterization, and simple rules to adapt the obtained probe-model parameters to the characteristics of the cable harness under test were derived. However, in both the above mentioned models the injection device is assumed to be clamped onto a single-ended interconnection and, as such, the practically relevant case of a wiring harness composed of multiple wires cannot be handled [6], [7]. A first attempt to extend the model can be found in [8]. However, the model there proposed still requires accurate knowledge of the probe interior [indeed, it extends the model in Fig. 1(a)], and it is suitable to differential lines only. To overcome these limitations, in this work a modeling procedure based on the second approach is proposed, and it is proven that probe-model parameters extracted from jig measurement can be easily adapted and successfully used for predicting BCI effects also in cable bundles composed of several wires. The procedure leads to a generalized Thévenin representation of the injection device

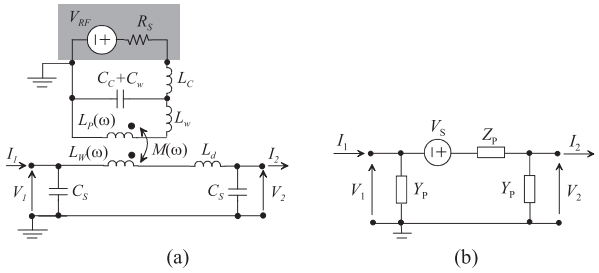

Fig. 1 Circuit model of the BCI probe clamped onto a single-wire interconnection [4]: (a) lumped-parameter circuit model; (b) equivalent probe-model seen from the wiring harness.

Manuscript received May 3, 2013.
Manuscript revised October 4, 2013.

[†]The authors are with the Department of Electronics, Information, and Bioengineering, Politecnico di Milano, P.za Leonardo da Vinci, 32, I-20133 Milano, Italy.
a) E-mail: flavia.grassi@polimi.it

DOI: 10.1587/transcom.E97.B.424

Copyright © 2014 The Institute of Electronics, Information and Communication Engineers

mounted onto the wiring harness. Such a lumped-parameter representation can be readily implemented into SPICE by behavioral components, and used for accurate prediction on condition that the probe width is electrically-short. In the frequency interval foreseen by BCI Standards (i.e., up to 400 MHz), most of the marketed BCI probes satisfies this condition. Without loss of generality, the analysis will focus on a wiring structure composed of two wires running parallel to ground, and terminated in (potentially) unbalanced circuit networks. Probe-model parameters will be extracted from the measurement data obtained on the calibration jig, and adapted to the characteristics of the cable harness under analysis by means of 2D numerical simulations. The obtained model will be then implemented into the SPICE environment and used to predict common mode (CM) and differential mode (DM) voltages induced at the line terminals. Model accuracy will be validated by 3D EM simulations carried out by CST Microwave Studio, [9].

2. Probe-Model Parameters

2.1 Extraction from Jig Measurement

In this Section, probe-model parameters V_S, Z_P, Y_P are retrieved from the measurement data obtained by mounting the injection device onto the calibration jig. To this end, an injection probe FCC F-130A [10] was mounted onto a calibration jig FCC BCICF-1 [10] as shown in Fig. 2(a), and the obtained structure was characterized at the three ports (see Fig. 2 for port numbering) by means of a Vector Network Analyzer (VNA) Agilent E5070B. Measurements were carried out in the frequency interval from 300 kHz to 400 MHz, and led to a 3×3 scattering parameter (SP) matrix in the form:

$$\mathbf{S} = \begin{bmatrix} S_{11} & S_{12} & S_{13} \\ S_{12} & S_{11} & -S_{13} \\ S_{13} & -S_{13} & S_{33} \end{bmatrix}, \tag{1}$$

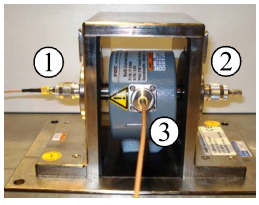

(a)

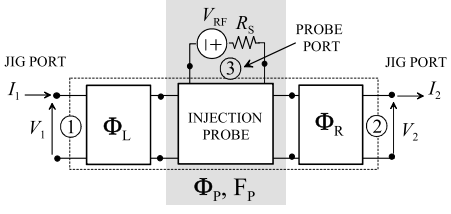

(b)

Fig. 2 Extraction of probe-model parameters from jig measurement: Picture (a) and principle drawing (b) of the experimental setup.

where subscript 3 denotes the input port of the probe, and subscripts 1, 2 refer to jig terminations. In order to obtain a two-port representation at the jig ports, port no.3 was eliminated by assuming a radio-frequency (RF) signal generator with parameters V_{RF}, $R_S = 50\,\Omega$, [gray block in Fig. 2(b)] connected with such a port, and by enforcing the corresponding port-constraints to port no.3 [4]. Conversion of the obtained SP representation into chain-parameter notation allowed expressing the relationships between voltages and currents at the jig ports as function of measurement data as:

$$\begin{pmatrix} V_2 \\ I_2 \end{pmatrix} = \mathbf{\Phi}_m \cdot \begin{pmatrix} V_1 \\ I_1 \end{pmatrix} + \mathbf{F}_m, \tag{2}$$

where $\mathbf{\Phi}_m$, $\mathbf{F}_m$ depend on the SPs in (1), and on the internal resistance (R_S) of the RF source. Subsequent interpretation of the overall structure as the cascade connection of three two-port networks, Fig. 2(b), allowed extracting a black-box model of the probe (inner active two-port) by de-embedding from measurement data ($\mathbf{\Phi}_m$, $\mathbf{F}_m$) those effects which are due to jig terminations (lateral blocks labeled by $\mathbf{\Phi}_L, \mathbf{\Phi}_R$), e.g., the time delay introduced by the taper terminations of the jig as well as reflections and field scattering at the interface between the inner conductor and the coaxial terminations of the jig. To this end, the jig circuit model developed and experimentally validated in [5] was used to evaluate the entries of the chain-parameter matrices $\mathbf{\Phi}_L$, $\mathbf{\Phi}_R$ modeling jig terminal sections. This finally allowed to extract V_S, Z_P, Y_P in Fig. 1(b) from the obtained matrix $\mathbf{\Phi}_P$ and vector $\mathbf{F}_P$ by solution of the matrix system:

$$\mathbf{\Phi}_P = \mathbf{\Phi}_R^{-1} \cdot \mathbf{\Phi}_m \cdot \mathbf{\Phi}_L^{-1} = \begin{bmatrix} 1 + Z_P Y_P & -Z_P \\ -Y_P(2 + Z_P Y_P) & 1 + Z_P Y_P \end{bmatrix}, \tag{3}$$

$$\mathbf{F}_P = \mathbf{\Phi}_R^{-1} \cdot \mathbf{F}_m = \begin{pmatrix} 1 \\ -Y_P \end{pmatrix} V_S. \tag{4}$$

Although effects due to jig terminations were preliminary de-embedded from measurement data, the parameters extracted from (3), (4) still incorporate contributions due to EM interaction between the probe and the inner wire of the calibration jig. However, circuit interpretation of these parameters by the light of the probe model in Fig. 1(a) allows to draw useful conclusions on the sensitivity of V_S, Z_P, Y_P on probe-to-wire interaction, as shown in the following subsection.

2.2 Variability with Cable Characteristics

In Fig. 1(b), the voltage source V_S and the impedance Z_P represent the parameters of the Thévenin equivalent circuit seen from the clamped conductor when looking towards the injection device. Frequency behavior of these parameters is strictly related to the frequency response of the probe ferrite core and to the specific arrangement of the probe primary winding, while it is marginally influenced by the characteristics of the cable harness clamped by the injection device. This is definitely true for V_S, whose invariability with

the characteristics of the clamped cable was experimentally proven in [5]. Conversely, impedance Z_P can be conveniently re-written as the sum of two terms, i.e.,

$$Z_P = \tilde{Z}_P + Z_d. \tag{5}$$

In (5), $\tilde{Z}_P$ does not depend on the characteristics of the wiring harness, and can be interpreted as the equivalent impedance seen from the clamped conductor when looking from the outlets of $\hat{L}_W(\omega)$. Contribution of such an impedance is dominant as long as the relative permeability of the ferrite core takes values much larger than one (i.e., in the lower frequency range). The second impedance $Z_d = j\omega L_d$ accounts for the portion of magnetic flux that leaks out the core without linking the clamped conductor. This leakage impedance — appreciably contributing to Z_P at high frequency — is inherently related to the characteristics of the clamped conductor, and needs to be calculated from time to time depending on the specific characteristics of the cable harness. Conversely, the portion of Z_P not influenced by probe-to-wire interaction ($\tilde{Z}_P$) can be evaluated from the impedance Z_P obtained by jig measurements by de-embedding the contribution of Z_d — here strictly related to the characteristics of the jig inner conductor — as: $\tilde{Z}_P \cong Z_P - j\omega L_{d,jig}$. To this end, the leakage inductance $L_{d,jig}$ is evaluated as the total inductance of the coaxial transmission-line (TL) section composed of the inner conductor of the jig (signal line) and the inner surface of the probe ferrite core. For probe FCC F-130A and jig FCC BCICF-1, this yields $L_{d,jig} \cong 11$ nH. In a similar fashion, also admittance $Y_P = j\omega C_S$ is related to probe-to-wire interaction only. Indeed, it accounts for capacitive coupling between the inner conductor of the jig and the probe metallic frame, which is kept at the same potential of the reference ground through the shields of the coaxial connectors (for the probe and jig here considered: $C_S \cong 6$ pF). As a consequence, clamping the probe onto a wiring harness requires to re-evaluate L_d and C_S only, starting from the geometry and material properties of the clamped conductor. From these considerations, probe-model extension shall involve (a) generalization and evaluation of the parameters associated with probe-to-wire interaction (i.e., L_d, C_S) and (b) combination of these parameters with those accounting for the probe frequency-response only (i.e., V_S and $\tilde{Z}_P$).

3. Probe-Model Extension

In this Section, it will be shown how probe-model parameters extracted from jig measurement can be used for effective prediction of BCI effects in multi-wire cable bundles. Although the analysis here presented will refer to a wiring structure composed of two wires running above ground, model generalization to cable bundles composed of more than two wires is straightforward.

3.1 Chain-Parameter Representation

For model derivation, the injection probe clamped on a two-wire interconnection above ground is modeled by an active four-port network, characterized in terms of chain parameters by a 4×4 matrix $\mathbf{\Phi}_P$, and a 4×1 vector $\mathbf{F}_P$. This extends the two-port representation in (3), (4) and Fig. 2(b), and allows for the circuit interpretation in Fig. 3, where: (a) two ideal voltage sources in series with the two wires represent the active part of the model, and (b) the 2×2 matrices $\mathbf{Z}_P$, $\mathbf{Y}_P$ are used to model the effect of loading and capacitive coupling exerted by the probe on the cable harness. In line with this representation, voltages and currents by the sides of the probe are related by:

$$\begin{pmatrix}\mathbf{V}_b\\ \mathbf{I}_b\end{pmatrix}=\begin{bmatrix}\mathbf{1}_2+\mathbf{Z}_P\mathbf{Y}_P & -\mathbf{Z}_P\\ -\mathbf{Y}_P(2\mathbf{1}_2+\mathbf{Z}_P\mathbf{Y}_P) & \mathbf{1}_2+\mathbf{Y}_P\mathbf{Z}_P\end{bmatrix}\cdot\begin{pmatrix}\mathbf{V}_a\\ \mathbf{I}_a\end{pmatrix}+\begin{pmatrix}\mathbf{V}_S\\ -\mathbf{Y}_P\mathbf{V}_S\end{pmatrix} \tag{6}$$

where $\boldsymbol{I}_2$ is the 2×2 identity matrix, $\mathbf{V}_{a(b)} = [V_{1a(b)} \;\; V_{2a(b)}]^T$, $\mathbf{I}_{a(b)} = [I_{1a(b)} \;\; I_{2a(b)}]^T$, $\mathbf{V}_S = [V_{S1} \;\; V_{S2}]^T$.

3.2 Model-Parameters Extracted from Measurement

To show how the parameters of the probe-model in Fig. 3 can be correlated to those extracted from jig measurement, we resort to the lumped-parameter circuit network in Fig. 4 [8], which extends the probe-model in Fig. 1(a). In this model, inductive coupling between the probe and the cable harness is represented by three coupled inductors with complex and frequency-dependent inductances, whereas two lumped-Π capacitive networks are used to model capacitive coupling. By this circuit interpretation, matrix $\mathbf{Z}_P$ and vector $\mathbf{V}_S$ can be evaluated as the parameters of the generalized Thévenin equivalent circuit seen from the cable harness looking towards the probe primary circuit. Accordingly, denoting as

$$V_{ab} = [1 + j\omega(R_S + j\omega L_C)(C_C + C_w)]^{-1} V_{RF} \tag{7}$$

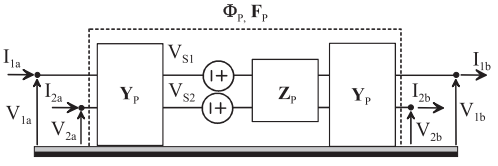

Fig. 3 Four-port representation of the BCI probe clamped onto a two-wire cable harness above ground.

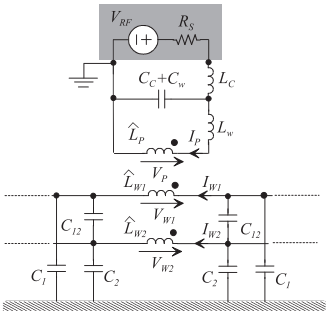

Fig. 4 Circuit model of the BCI probe clamped onto a two-wire cable harness above ground [8].

$$Z_{ab} = j\omega L_w + \frac{R_S + j\omega L_C}{1 + j\omega(R_S + j\omega L_C)(C_C + C_w)} \tag{8}$$

the parameters of the Thévenin equivalent of the probe primary circuit seen from the outlets of $\hat{L}_P$, and as

$$\begin{pmatrix} V_P \\ V_{W1} \\ V_{W2} \end{pmatrix} = j\omega \hat{\mathbf{L}}_f \cdot \begin{pmatrix} I_P \\ I_{W1} \\ I_{W2} \end{pmatrix}; \quad \hat{\mathbf{L}}_f = \begin{bmatrix} \hat{L}_P & \hat{M}_{P1} & \hat{M}_{P2} \\ \hat{M}_{P1} & \hat{L}_{W1} & \hat{M}_{12} \\ \hat{M}_{P2} & \hat{M}_{12} & \hat{L}_{W2} \end{bmatrix} \tag{9}$$

the port-constraints enforced by the coupled inductors $\hat{L}_P$, $\hat{L}_{W1}$, $\hat{L}_{W2}$, matrix $\mathbf{Z}_P$ and vector $\mathbf{V}_S$ take the form:

$$\mathbf{Z}_P = j\omega \begin{bmatrix} \hat{L}_{W1} - \frac{\hat{M}_{P1}^2}{\hat{L}_T} & \hat{M}_{12} - \frac{\hat{M}_{P1}\hat{M}_{P2}}{\hat{L}_T} \\ \hat{M}_{12} - \frac{\hat{M}_{P1}\hat{M}_{P2}}{\hat{L}_T} & \hat{L}_{W2} - \frac{\hat{M}_{P2}^2}{\hat{L}_T} \end{bmatrix} \tag{10}$$

$$\mathbf{V}_S = -\begin{pmatrix} \hat{M}_{P1} \\ \hat{M}_{P2} \end{pmatrix} \frac{V_{ab}}{\hat{L}_T}, \tag{11}$$

where $\hat{L}_T = \hat{L}_P + Z_{ab}/(j\omega)$.

To evaluate the entries of $\mathbf{Z}_P$, $\mathbf{V}_S$ in (10), (11), self and mutual inductances in (9) are expressed in terms of (a) reluctance of the ferrite-core, $\hat{\Re}(\omega)$, and (b) number of turns of the probe primary winding, N_P, as

$$\hat{\mathbf{L}}_f = \begin{bmatrix} N_P^2/\hat{\Re}(\omega) & N_P/\hat{\Re}(\omega) & N_P/\hat{\Re}(\omega) \\ N_P/\hat{\Re}(\omega) & 1/\hat{\Re}(\omega) + L_{d1} & 1/\hat{\Re}(\omega) + M_d \\ N_P/\hat{\Re}(\omega) & 1/\hat{\Re}(\omega) + M_d & 1/\hat{\Re}(\omega) + L_{d2} \end{bmatrix}, \tag{12}$$

where L_{d1}, L_{d2}, M_d account for the portion of flux which does not link the wires clamped by the probe. Indeed, these inductances extend the concept of leakage inductance L_d in Fig. 1(a), and require to be evaluated starting from the characteristics of the clamped conductor, as it will be shown in the following sub-section. Once leakage inductances L_{d1}, L_{d2}, M_d are known, some simple algebra (here omitted for brevity) allows expressing $\mathbf{Z}_P$ and $\mathbf{V}_S$ in (10), (11) as function of the parameters extracted from jig measurements (i.e., impedance $\tilde{Z}_P$, and voltage source V_S) as

$$\mathbf{Z}_P = \tilde{Z}_P \begin{bmatrix} 1 & 1 \\ 1 & 1 \end{bmatrix} + j\omega \underbrace{\begin{bmatrix} L_{d1} & M_d \\ M_d & L_{d2} \end{bmatrix}}_{\mathbf{L}_d} = \tilde{\mathbf{Z}}_P + \mathbf{Z}_d \tag{13}$$

$$\mathbf{V}_S = V_S \begin{pmatrix} 1 \\ 1 \end{pmatrix} = V_S \mathbf{1}_{2\times 1}. \tag{14}$$

It's worth noting that the formulation in (13), (14) allows to readily account for the frequency-dependent behaviour of the probe core without requiring accurate information on the probe interior. Additionally, it can be easily generalized to handle cable bundles composed of N (with $N > 2$) wires, at the cost of re-evaluating matrices $\mathbf{Z}_d$, and $\mathbf{Y}_P$ as explained in the following.

3.3 Model-Parameters Requiring *ad hoc* Evaluation

Probe-model parameters requiring *ad hoc* evaluation are those accounting for probe-to-wire interaction, that is matrices $\mathbf{Z}_d = j\omega\mathbf{L}_d$ and $\mathbf{Y}_P = j\omega\mathbf{C}_S$ in (6), (13). With reference to the cross-section view in Fig. 5, the entries of the inductance matrix $\mathbf{L}_d$ can be interpreted and calculated as the total self and mutual inductances of the coaxial TL section composed of the clamped conductors (signal lines), and the inner surface of the probe ferrite core, which here behaves as an equivalent shield with radius r_c. For widely-separated wires [11], approximate analytical expressions of the involved per-unit-length (p.u.l) inductances can be found in [11, Sect. 9.3]. For close conductors, numerical simulation of the involved 2D cross-section is required in order to calculate such p.u.l. inductances. The entries of matrix L_d can be then evaluated by multiplying the obtained p.u.l. inductances by the probe longitudinal width, $\mathscr{L}_P$, (e.g., for probe FCC F-130A, $\mathscr{L}_P \cong 63$ mm). In a similar fashion, the entries of the stray-capacitance matrix $\mathbf{C}_S$ can be evaluated by interpreting the two wires and the inner surface of probe-hole as a coaxial TL section, where the wires behave as signal lines, and the inner surface of the probe metallic frame behaves as an ideal shield with radius r_f (see Fig. 5). The involved p.u.l. capacitances can be calculated by analytical expressions [11, Sect. 9.3], or by 2D electrostatic simulation, depending on wires separation and on the absence/presence of dielectric jackets around the wires. The obtained p.u.l. capacitances are then multiplied by half the probe longitudinal width, $\mathscr{L}_P$, since in the proposed model capacitive coupling is symmetrically distributed by the two sides of the probe.

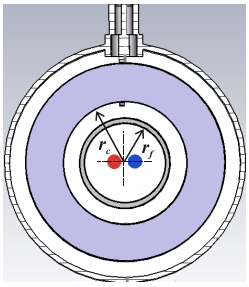

Fig. 5 Cross-section view of the BCI probe clamping a two-wire cable harness. For probe FCC F-130A: $r_f \approx 16$ mm, $r_c \approx 24$ mm, [4].

It's worth to note that these calculations do not require information on the probe interior. Indeed, r_f, r_c and $\mathscr{L}_P$ can be easily measured from the probe exterior, or even found in probe data-sheets.

4. Circuit and Electromagnetic Simulation

As a specific example, the proposed probe model is here used to predict the noise induced by BCI at the terminations of a two-wire structure. This example is of significant interest from the communications viewpoint, since several communication protocols make use of physical layers involving differential-line buses (e.g., twisted-wire pair cables) to ensure signal immunity to EM interference [3]. Indeed, in these structures the interference pick-up (both radiated and conducted) is mainly determined by noise-rejection and CM to DM conversion characteristics of the terminal units. As a consequence, the current levels assigned by BCI Standards

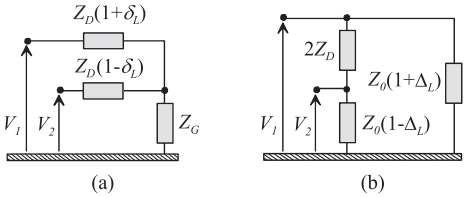

Fig. 6 Lumped-Tee (a) and lumped-Π (b) circuit networks used to model not-perfectly balanced terminal units (right-end side).

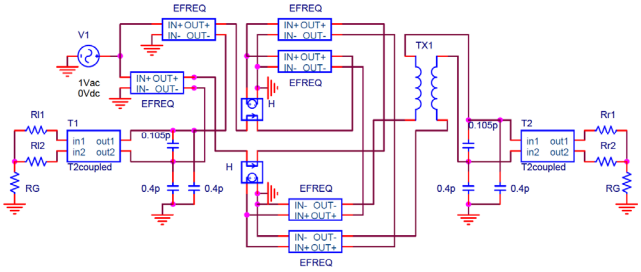

Fig. 7 SPICE schematic modeling the BCI setup under analysis.

and enforced by probe calibration on the jig (i.e., the bulk CM current flowing through the harness) have scarce correlation with the DM noise actually stressing the terminal units during the injection test. Despite that, this example (corroborated by 3D simulations) will show that extracting probe-model parameters from jig measurements and combining them with specific parameters calculated by simple 2D simulations (see Sect. 3.3) suffices to reproduce the CM-to-DM conversion phenomenon at the basis of terminal units susceptibility, and to accurately predict both CM and DM disturbance at the line terminals.

4.1 Two-Wire Structure under Analysis

Without loss of generality, a well-balanced wiring structure composed of a pair of 25 cm long bare and lossless parallel conductors running above a perfect ground plane is here considered. Wire length is $\mathscr{L} = 25\,\text{cm}$, wire radius is $r_w = 0.4\,\text{mm}$, wire separation is $s = 8\,\text{mm}$, wire height above ground is $h = 50\,\text{mm}$. For the purpose of this analysis, such an interconnection is assumed to be terminated in potentially unbalanced terminal units, which can be equivalently represented by the lumped-Tee or lumped-Π circuit networks in Fig. 6. In these networks, coefficients δ_X [Fig. 6(a)] and Δ_X [Fig. 6(b)] are used to include into the model possible imbalance due to the left (subscript $X = S$) and right (subscript $X = L$) terminal units. Additionally, in line with typical design strategies of differential lines (aimed at enhancing DM signaling while increasing immunity to conducted/radiated noise), the input impedance of the terminal units ($2Z_D$) is assumed to be matched to the DM characteristic impedance, Z_{DM}, of the wiring harness. For the lossless and bare TL structure here considered, the DM impedance Z_{DM} can be expressed as function of the p.u.l. self and mutual inductances ℓ_s, ℓ_m as

$$Z_{DM} \cong 2c_0\ell_s(1 - \ell_m/\ell_s), \tag{15}$$

where c_0 denotes the light-speed in free-space. Therefore, enforcing the matching condition $Z_{DM} = 2Z_D$ leads to the value $Z_D \cong 179\,\Omega$ for the load impedances in Fig. 6.

4.2 Circuit Simulation (SPICE)

For prediction of modal voltages at the line terminals, injection probe FCC F-130A was assumed to be clamped on the two-wire structure described in Sect. 4.1 at midpoint. The whole injection setup was implemented and simulated by SPICE, and CM and DM voltages were retrieved from the voltages V_1, V_2 obtained at the line right-end as: $V_{CM} = (V_1 + V_2)/2$, $V_{DM} = V_1 - V_2$. The SPICE schematic used for circuit simulation is shown in Fig. 7. In this network, line terminations in Fig. 6(a) were modeled by resistors, and line sections by the sides of the probe were modeled by two three-conductor TLs with length $\mathscr{L}_S = (\mathscr{L} - \mathscr{L}_P)/2 \cong 93.5\,\text{mm}$. In SPICE, this was achieved by the use of two **T2coupled** parts (**Tline** library) with $\ell_S \cong 1.1\,\mu\text{H/m}$, $\ell_m \cong 0.5\,\mu\text{H/m}$, $c_S \cong 12.8\,\text{pF/m}$, $c_m \cong -5.85\,\text{pF/m}$. Concerning the probe model, the frequency-dependent entries of the impedance matrix $\tilde{\mathbf{Z}}_P$ and the source vector $\mathbf{V}_S$ (i.e., those probe-model parameters which were extracted from jig measurement in Sects. 2.1 and 3.2) were implemented in SPICE by recourse to the ABM (Analog Behavioral Model) part **EFREQ**. This part allows to include measurement data into the simulation environment, as it behaves as a voltage-controlled voltage source with gain assigned frequency-by-frequency by means of a look-up table. Accordingly, in Fig. 7 the two **EFREQ** parts connected with the ac voltage source are used to model the induced voltage sources $V_{S1} = V_{S2} = V_S$ in Fig. 3. In a similar fashion, the entries of matrix $\tilde{\mathbf{Z}}_P$ in (13) are implemented by appropriate connection of four **EFREQ** parts with suitable current-controlled (**H** parts in Fig. 7) voltage sources with unitary gains. Such a behavioral model is then augmented by additional circuit components accounting for probe-to-wire interaction. Namely, a pair of coupled inductors (part **TX1**), with self-inductances $L_{d1,2} \cong 51\,\mu\text{H}$ and coupling coefficient $k \cong 0.28$ is used to model matrix $\mathbf{Z}_d$ in (13). Two lumped-Π capacitive networks, each comprising a wire-to-wire capacitor of 0.105 pF, and a couple of wire-to-ground capacitors of 0.4 pF, are used to model matrices $\mathbf{Y}_P$ in (6). These values were evaluated by 2D numerical simulation (carried out by the commercial software Maxwell 2D) of the equivalent coaxial-cable cross-sections introduced in Sect. 3.3, which only involve geometrical data (i.e., r_f, r_c, and L_P) that can be easily measured from the probe exterior.

4.3 EM Simulation (CST Microwave Studio)

To corroborate the predictions obtained by SPICE simulation, the two-wire injection setup in Sect. 4.1 is modeled by the Finite Integration Technique (FIT)-based code CST Microwave Studio (MWS), [9]. The wiring structure im-

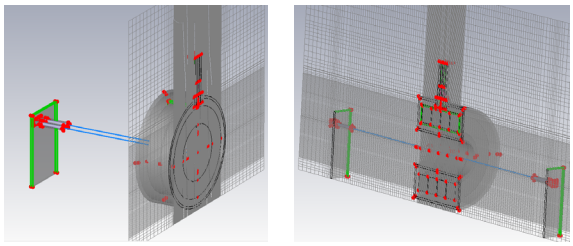

Fig. 8 EM model of injection probe FCC F-130A mounted onto a two-wire test fixture: Detailed view of the 5000000 hexahedral-cells mesh used for numerical simulation in CST MWS, [9].

plemented for full-wave 3D simulation (see Fig. 8) resembles the single-ended test fixture used in [4]. Indeed, two vertical metallic strips soldered to a metallic ground plane, each hosting a pair of SMA pass-through connectors, are introduced to host the two wires and to allow for connection with the so-called *wave-guide ports* available in CST MWS. Injection probe FCC F130-A is clamped onto the fixture at midpoint. Its EM model includes the metallic frame, the toroidal ferrite core, the primary winding (i.e., the wire wound around the ferrite core), and the input connector/adapter pair used for experimental characterization of the probe via VNA measurement [the effects due to this additional adapter are inherently included into the parameters $\tilde{Z}_P$, V_S extracted from jig measurement, see Fig. 2(a)]. The metallic frame and the primary winding are made of perfect electric conductor (PEC), whereas both PEC and dielectrics are used for modeling the input connector/adapter series. Four insulated rings with user-defined material-properties are used to reproduce the frequency response of the probe ferrite core. Ferrite relative permittivity was set to ε_r = 14. Ferrite relative permeability (μ_r) was represented by a Debye model, whose parameters (i.e., static value 375, and time constant 0.5 ns) were tuned by iterative simulations aimed at reproducing the measured input-impedance, [12]. This repetitive procedure was used for an *a posteriori* characterization of the ferrite intrinsic properties, which could not be directly extracted from input impedance measurement due to superposition with high-frequency phenomena occurring within large ferrite cores. These phenomena — e.g., eddy currents and dimensional resonances originating from non-uniform distribution of the magnetic flux on the core surface [13] — require accurate meshing of the probe core in order to be effectively reproduced by EM simulation. Therefore, to achieve accurate prediction, simulations were carried out in a bounding box of length 400 mm, depth 400 mm, and width 250 mm with an adaptive mesh of 5000000 hexahedral-cells (see in Fig. 8). To emulate free-space conditions, open boundary conditions (PML in CST MWS) were assigned to all box faces, with the exception of the bottom face, where electric boundary conditions (which set at zero the tangential component of the electric field vector) were imposed to mimic the presence of a perfect ground plane.

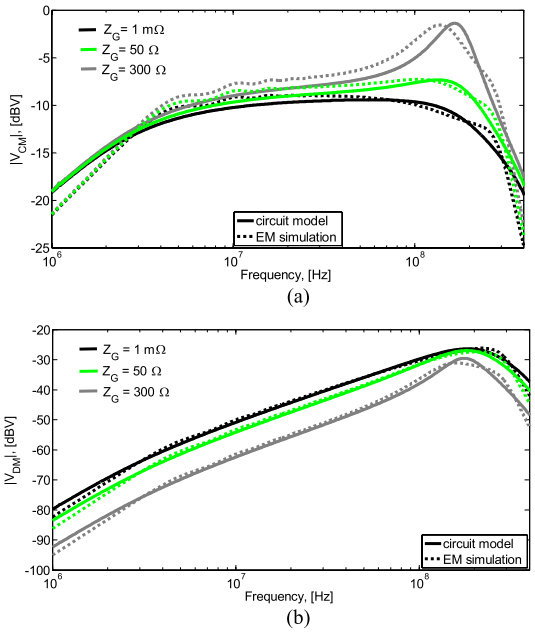

Fig. 9 CM(a) and DM (b) voltage prediction at the right line-end for different values of the impedance Z_G: SPICE (solid curves) versus CST MWS (dotted curves) simulation ($\delta_S = \delta_L = 0.1$).

4.4 Prediction of Modal Voltages

CST MWS simulations were carried out from 1 up to 400 MHz, by connecting a wave-guide port (emulating the coaxial port of a VNA) to each of the five ports of the injection setup. The obtained five-port SP representation — which does not depend on the terminal networks — was firstly reduced by assuming a non-ideal RF voltage source with internal parameters V_{RF}, $R_S = 50\,\Omega$ connected with the probe input, and then converted into chain-parameter representation. Modal voltages at the right termination of the setup were finally evaluated by enforcing the port constraints imposed by the terminal networks in Fig. 6(a). The obtained modal voltages (dotted curves) are compared with the predictions obtained by SPICE simulation (solid curves) in Fig. 9 and Fig. 10. For the sake of comparison, the SPICE model (see Sect. 4.2) was preliminary augmented by suitable lumped-parameter circuit networks modeling the effects due to the SMA connectors and vertical strips exploited for 3D simulation. This was achieved by extending to the two-wire structure in Fig. 8 the circuit models developed for the single-ended test fixture in [4].

In the first figure (Fig. 9), (a) CM and (b) DM voltages induced at the right termination are plotted for three different values of the grounding impedance Z_G (here, equal degree of unbalance at both the line terminals, i.e., $\delta_S = \delta_L$ = 0.1, was set). In the second figure (Fig. 10), the dependence of DM voltages on the degree of unbalance of the terminal networks is investigated by considering three different combinations of coefficients δ_S, δ_L (in this case, all the plotted curves were obtained with $Z_G = 1\,\mathrm{m}\Omega$). The correspond-

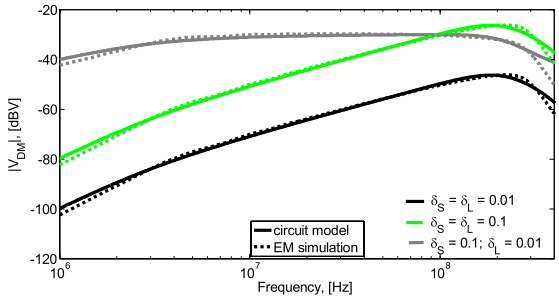

Fig. 10 DM voltage prediction at the right line-end for different degrees of unbalance of the terminal networks: SPICE (solid curves) versus CST MWS (dotted curves) simulation ($Z_G = 1\,\mathrm{m}\Omega$).

ing plot for CM voltages is here omitted, since CM voltages are scarcely influenced by termination unbalance. In particular, for the specific values of δ exploited in Fig. 10, no appreciable variations of CM voltages were observed. On the whole, a remarkable agreement is observed between the curves obtained by circuit (SPICE) and EM (CST MWS) simulation. In-band differences on the order of 1 or 2 dB are to be ascribed partly to the approximations involved in the circuit model of the terminations of the test fixture (i.e., SMA connectors and vertical strips used for 3D EM simulation), and partly to the fact that the EM simulation itself has finite precision. In particular, the small oscillations observed in Fig. 9(a) at low frequency can be explained by recalling that the EM software used for EM simulation resorts to a time-domain solver.

5. Conclusion

The standard procedure for BCI probe calibration is based on the use of an electrically short, ideally matched single-ended test fixture, i.e., the so-called jig. However, application of the BCI technique to real systems often shows that the actual RF levels injected into the terminal units of the system under test may largely differ from the expected levels, [3]. This originates from the substantial difference between the single-ended 50 Ω ideal structure of the jig and the multi-wire (and thus multi-mode) nature of real cable harnesses with arbitrary terminations. This issue is well exemplified by systems involving differential lines for data transmission, whose conducted and radiated immunity properties are severely affected by the noise-rejection and mode-conversion characteristics of the terminal units. However, these aspects are left out of the BCI calibration procedure which, resorting to the jig, can only provide rough estimates of the injected CM noise current. Despite the aforementioned limitations, it is possible to show that experimental characterization of the injection probe mounted onto the calibration jig can be used to extract an equivalent circuit model of the probe allowing for precise description of the injection phenomenon, and for accurate prediction of the conducted immunity of terminal units connected through multi-wire structures. This was done in this paper by recourse to circuit and EM modeling of a BCI test setup involving a differential line above ground with simple but not ideal terminations. The proposed modeling procedure, which does not require accurate knowledge on the probe interior, leads to a measurement-based behavioral model which can be easily implemented into the SPICE environment via behavioral parts. One of the key features of this model is that it can be easily adapted to multi-wire harnesses with different characteristics by setting the values of few circuit elements accounting for EM interaction between the probe and the wiring harness. Accordingly, even if the results here shown were derived for a two-wire structure, model extension to a cable harness composed of an arbitrary number of wires is straightforward.

References

[1] D.A. Hill, "Currents induced on multiconductor transmission lines by radiation and injection," IEEE Trans. Electromagn. Compat., vol.34, no.4, pp.445–450, Nov. 1992.
[2] M. Klingler, M. Szelag, and M. Heddebaut, "Double bulk current injection: A possible substitute to field-to-wire coupling," Proc. EUROEM'94, pp.1249–1256, Bordeaux, France, 1994.
[3] C. Rostamzadeh and S.A. Pignari, "Test procedure for CAN bus susceptibility evaluation based on the use of radio frequency detectors," Proc. XIXth URSI General Assemby, Chicago, IL, Aug. 2008.
[4] F. Grassi, F. Marliani, and S.A. Pignari, "Circuit modeling of injection probes for bulk current injection," IEEE Trans. Electromagn. Compat., vol.49, no.3, pp.563–576, Aug. 2007.
[5] F. Grassi and S.A. Pignari, "Characterization of the bulk current injection calibration-jig for probe-model extraction," Proc. 2010 IEEE Int. Symp. on Electromagn. Compat., pp.344–347, Fort Lauderdale, FL, USA, July 2010.
[6] C.Y. Ho, C.H. Huang, and T.S. Horng, "Conducted susceptibility diagnosis of vehicle electronic module using correlation between mixed-mode S-parameter measurement and bulk current injection test," Proc. ASID 2009, pp.635–638, Hong Kong, China, Aug. 2009.
[7] K. Sasabe, K. Yoshida, A. Bullivant, and O. Fujiwara, "Experimental investigation of noise immunity diagnosis for printed circuit boards by bulk current injection test," Proc. 1999 Int. Symp. Electromagn. Compat., pp.556–559, Tokyo, Japan, May 1999.
[8] F. Grassi and S.A. Pignari, "Bulk current injection in twisted wire pairs with not perfectly balanced terminations," IEEE Trans. Electromagn. Compat., Early access article, pp.1–9, April 2013, doi: 10.1109/TEMC.2013.2255295.
[9] CST Studio Suite, 2012. [Online] http://www.cst.com/
[10] Fischer Custom Communications, [Online] http://www.fischercc.com/
[11] C.R. Paul, Introduction to Electromagnetic Compatibility, Wiley-Interscience, New York, 2006.
[12] L. Di Rienzo, F. Grassi, and S.A. Pignari, "FIT modeling of injection probes for bulk current injection," Proc. ACES 2007, pp.782–787, Verona, Italy, 2007.
[13] E.C. Snelling, Soft ferrites: properties and applications, Iliffe Books, London, U.K., 1969.

Flavia Grassi received the Laurea and Ph.D. degrees in electrical engineering from the Politecnico di Milano, Italy, in 2002 and 2006, respectively, where she has been an Assistant Professor since 2008. From 2008 to 2009, she was with the European Space Agency (ESA), The Netherlands. Her research interests are focused on the characterization of measurement setups for electromagnetic compatibility testing (aerospace and automotive sectors), and applications of the powerline communications (PLC) technology on ac and dc lines.

Giordano Spadacini received the Laurea and Ph.D. degrees in electrical engineering from the Politecnico di Milano, Milan, Italy, in 2001 and 2005, respectively. Since 2007 he has been an Assistant Professor at the Politecnico di Milano, Department of Electronics, Information and Bioengineering. His research interests include distributed-parameter circuit modeling, statistical models for the characterization of interference effects, and EMC in railway and aerospace systems. Dr. Spadacini received the IEEE EMC Transactions Prize Paper Award for the best paper published in 2004.

Sergio A. Pignari received the Laurea and Ph.D. degrees in electronic engineering from the Politecnico di Torino, Turin, Italy, in 1988 and 1993, respectively. From 1991 to 1998, he was an Assistant Professor with the Department of Electronics, Politecnico di Torino. In 1998, he joined Politecnico di Milano, Milan, Italy, where he is currently a Full Professor of Circuit Theory and Electromagnetic Compatibility (EMC) with the EMC Group, at the Department of Electronics, Information, and Bioengineering. He is the author or coauthor of more than 130 papers published in international journals and conference proceedings. His current research interests include characterization of interference effects, distributed parameter circuit modeling, statistical techniques for EMC, and experimental procedures and setups for EMC testing. Dr. Pignari was the recipient of the IEEE EMC Society 2004 Transactions Prize Paper Award. He is currently an Associate Editor of the IEEE Transactions on EMC and the IEEE EMC Society Chapter Coordinator.